2021 43rd Annual International Conference of the
IEEE Engineering in Medicine & Biology Society (EMBC)
Oct 31 - Nov 4, 2021. Virtual Conference

2D tissue strain tensor imaging in quasi-static ultrasound elastography*

Anne-Lise Duroy[1], Valérie Detti[1], Agnès Coulon[2], Olivier Basset[1], Elisabeth Brusseau[1]

Abstract - **Accurately estimating all strain components in quasi-static ultrasound elastography is crucial for the full analysis of biological media. In this paper, 2D strain tensor imaging is investigated, using a partial differential equation (PDE)-based regularization method. More specifically, this method employs the tissue property of incompressibility to smooth the displacement fields and reduce the noise in the strain components. The performance of the method is assessed with phantoms and *in vivo* breast tissues. For all the media examined, the results showed a significant improvement in both lateral displacement and strain but also, to a lesser extent, in the shear strain. Moreover, axial displacement and strain were only slightly modified by the regularization, as expected. Finally, the easier detectability of the inclusion/lesion in the final lateral strain images is associated with higher elastographic contrast-to-noise ratios (CNRs), with values in the range [0.68 - 9.40] vs [0.09 - 0.38] before regularization.**

I. Introduction

Over the past few decades, elastography techniques have been developed for the *in vivo* investigation of the mechanical properties of soft tissues [1-3]. This study focuses on quasi-static ultrasound elastography, which produces strain images of biological media under compression. Commonly, only the axial strain (along the acoustic beam) is estimated. However, some authors have shown that other components of strain could also provide useful information about the observed tissue. For instance, shear strain gives information about lesion mobility [4,5]. Various methods can be found in the literature that compute the different components of tissue displacement [6-8]. Nonetheless, ultrasound images are characterized by anisotropic resolution, which leads to coarser quality of fields for the displacement components orthogonal to the axial direction. This results in strain images highly affected by noise. Yet, accurately estimating all strain components remains crucial for fully analyzing a medium, not only through a more complete visualization of the tissue response, but also through implementation of further computational methods necessary to reconstruct mechanical parameters such as Young's modulus [9].

*This work was performed within the framework of the LABEX CELYA (ANR-10-LABX-0060/ANR-11-IDEX-0007) and LABEX PRIMES (ANR-11-LABX-0063/ANR-11-IDEX-0007). Ultrasound data acquisition was performed using equipment provided by PILoT, INSA-Lyon, France.

[1]Univ Lyon, INSA-Lyon, Université Claude Bernard Lyon 1, UJM Saint-Etienne, CNRS, Inserm, CREATIS UMR 5220, U1294, France

[2]Département de radiologie, Centre de lutte contre le cancer Léon Bérard, Lyon, France

Different methods have been introduced to improve displacement estimation, especially of lateral one. Some developments focus in particular on the data used for displacement computation. In [4,10], for instance, the displacement is determined from estimations performed along multiple insonification angles. In [11], Liebgott *et al.* propose the use of specific radiofrequency (RF) images more adapted to track the tissue lateral displacement than conventional ones. These RF images include lateral oscillations, resulting from a particular beamforming. Other work focuses instead on the estimation method itself to reduce noise in elastograms, notably with the development of regularization-based approaches [12-15]. Guo *et al.* [16] recently proposed a partial differential equation (PDE)-based regularization method to smooth the displacement fields using the (quasi) incompressibility property of soft tissues [17]. This method has shown promising results, especially with an important increase in the contrast-to-noise ratio (CNR) for lateral strain images.

In this paper, we investigate 2D strain tensor imaging and more particularly the improvement in strain images produced by complementing our motion-tracking approach [18] with the PDE-based regularization method [16]. The overall method we have developed works as follows: 1) both axial and lateral displacements are estimated with our motion-tracking technique, 2) the resulting displacement fields are then regularized, and 3) axial, lateral, and shear strain images are computed from the gradient of the estimated displacements. The performance of the method is assessed with phantom and *in vivo* breast data. Numerical models of the phantom experiments are also provided for a more thorough analysis of the estimated fields. Finally, a quantitative assessment of the method is carried out, with the computation of CNR values.

II. METHOD

A. Estimation of the displacement fields

As previously mentioned, a large variety of approaches are available to estimate the displacement fields from RF ultrasound images. The method developed by our group and used in this study is briefly explained here. We refer the reader to the following papers for additional information [18,19].

The basic principle of the method is the following: let us consider I_1 and I_2, two RF images acquired during medium deformation. First, I_1 is subdivided into multiple 2D regions of interest (ROIs) of the same dimensions,

regularly positioned and overlapping each other. Then, for each one of these ROIs, its deformed replica is identified in I_2 via the maximization of the correlation coefficient (CC). Contrary to most motion-tracking methods, where only a 2D shift is considered, an axial scaling factor α is also introduced to describe the ROI transformation between I_1 and I_2. This factor allows us to take into account the shape variations that occur in the RF signal due to the medium deformation. Along the lateral direction, however, scaling is ignored because of the coarser image resolution. Finally, the axial strain can be directly deduced from the scaling factor ($\varepsilon = \alpha - 1$) without requiring derivative computation. Note that the correlation coefficient provides an indication of the match achieved during parameter estimation, the closer the value to 1, the better is the match. In case of insufficient match ($CC < 0.75$), the estimates are labeled as untrustworthy and a local regularization is applied to ensure continuity with spatially close estimates characterized by $CC \geq 0.75$.

Typically in elastography, sequences of RF images are acquired. With our method, parameters are calculated between consecutive RF images, in order to limit errors due to out-of-plane motion. Indeed between two successive frames, it is expected that such motion will be lower than between the first and the last frames of the sequence. The final displacement fields and axial strain maps are then obtained by combining the contribution of all pairs of images. As will be illustrated in the Results section, this method enables to accurately estimate the axial displacement field but the lateral one remains generally too noisy to be used directly for strain computation.

B. Regularization

The second step consists in regularizing the previously estimated displacements using the (quasi) incompressibility property of tissues. Contrary to the regularization described in step 1, whose application is local, the one here is performed unconditionally over the whole image. Let $\bar{\boldsymbol{d}}$ be a displacement previously estimated in the domain Ω, whose axial and lateral components are $\bar{u}$ and $\bar{v}$, respectively. Regularized displacement fields u and v are obtained by minimizing an objective function F, as follows:

$$\underset{u,v}{\text{Minimize}} \quad F(u,v), \text{ with :}$$

$$F(u,v) = \int_\Omega (\nabla \cdot \boldsymbol{d})^2 + \lambda_1 \int_\Omega (u - \bar{u})^2 + \lambda_2 \int_\Omega (v - \bar{v})^2 \quad (1)$$

where λ_1 and λ_2 are the weighting coefficients. The first term of the objective function is the incompressibility condition, while the other two are the data fidelity terms. λ_1 and λ_2, which are both constant and positive, modulate the regularization weight on the fields.

The problem is solved using a similar approach to the one described in [16], where F is minimized via the gradient descent method and the Euler-Lagrange equations. Displacement derivatives are approximated using finite differences and the Neumann boundary condition at $\partial\Omega$, $\nabla \boldsymbol{d}\, \boldsymbol{n} = \boldsymbol{0}$, with $\boldsymbol{n}$ the outward normal at the boundary. λ_1 and λ_2 are tuned by visual inspection of the results to improve them in terms of noise reduction and inclusion/lesion detection. Lastly, the convergence criterion is chosen as :

$$\sqrt{\sum_{pixels} ((u^k - u^{k-1})^2 + (v^k - v^{k-1})^2)} < \xi \quad (2)$$

with u^k and v^k the axial and lateral displacements at iteration k, and $\xi = 10^{-8}$, considering that the results remain quasi-unchanged below this threshold. The fields are thus iteratively updated until the convergence criterion or the maximum number of iterations (here $N = 50,000$) is reached.

III. RESULTS AND DISCUSSION

An initial assessment of the method was carried out with breast phantoms, two *CIRS* models 059 (Computerized Imaging Reference Systems, Norfolk, VA, USA), and also with breast tissues *in vivo*. For each region examined, a typical quasi-static elastography experiment was performed, i.e., the medium was cautiously and continuously compressed and decompressed by the operator using the ultrasound probe while the RF images were acquired. Data were collected with an *Ultrasonix* ultrasound scanner equipped with an L14-5W/60 transducer. The sampling frequency was 40 MHz. In this paper, three examples of results are presented, with displacement and strain fields obtained during medium compression (cases #1 and #3) and decompression (case #2), for a more complete illustration.

Before detailing the results, a few comments on the choice of the weighting coefficients need to be made. First, it is interesting to note that the values of λ_1 and λ_2 were kept unchanged in all three cases, i.e., 10 and 0.03, respectively. This choice was made for λ_1 to prevent any loss of quality in the axial component of the displacement, and for λ_2 to allow for sufficient modifications in the lateral component. Indeed, large values of λ limit field variations, and with these weights, the regularization will mostly modify the lateral fields.

Two phantom results are first presented: one for a region containing a single inclusion (case #1, Fig. 1a, Fig. 2), and the other, two inclusions one above the other (case #2, Fig. 1b, Fig. 3). In both cases, the inclusions are approximately

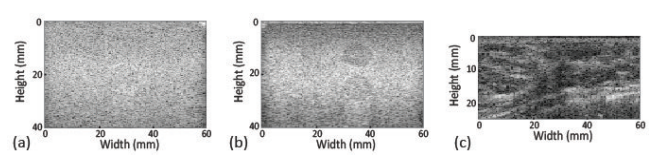

Fig. 1. B-mode images. From left to right: phantom - case #1, phantom - case #2, and *in vivo* breast tissues - case #3.

three times stiffer than the background (information provided by the manufacturer). For these two cases, a numerical model was built with *Comsol Multiphysics*® [20]. The simulations reproduce the configuration of 3D media containing inclusion(s) that are deformed using a transducer, with the applied displacement manually adjusted to obtain values similar to those measured experimentally. Although it is not possible to perfectly model the experiment, these simulations will provide elements to which the experimental results can be compared, such as the range of lateral strain values or shear strain patterns. This should help us to assess and analyze the experimental fields.

Results from case #1 are displayed in Fig. 2, and case #2 in Fig. 3. Although the second case comprises two inclusions spatially close, similar results can be observed. Unlike the axial displacement (a), the lateral one before regularization (d) is noisy, and cannot provide useful information about the phantom lateral strains (m). However, both displacements remain in agreement with the simulations (c,f). After regularization, the lateral displacement (e) is smoother compared with (d). This smoothing is sufficient to significantly enhance the lateral strain (n), resulting in an image where the inclusions are clearly revealed. Moreover, the lateral strain field (n) is consistent with its corresponding simulated field (o), and exhibits the same range of strain values, which was not the case before. Indeed, before regularization, the lateral strain (m) is highly affected by noise, leading to a much wider range of values.

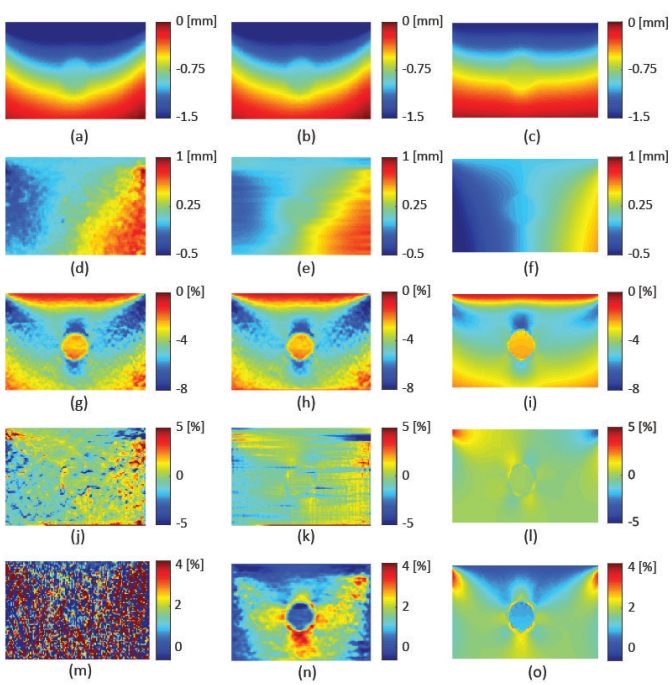

Fig. 2. Phantom results - case #1. From top to bottom: axial displacement, lateral displacement, axial strain, shear strain, and lateral strain. From left to right: fields before regularization, after regularization, and simulated. A 8×2 median filter was used in (j) and (k).

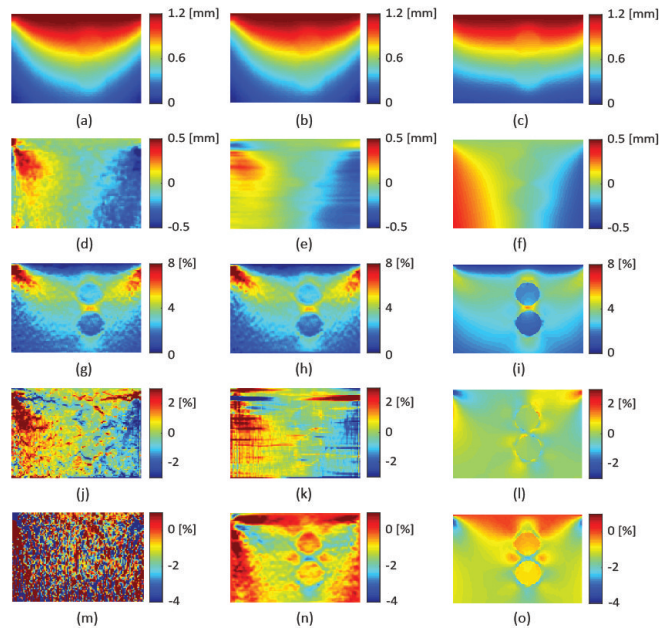

Fig. 3. Phantom results - case #2. From top to bottom: axial displacement, lateral displacement, axial strain, shear strain, and lateral strain. From left to right: fields before regularization, after regularization, and simulated. A 8×2 median filter was used in (j) and (k).

By contrast, the regularization has no visible impact on the axial displacement (a,b), and thus on the axial strain (g,h), as expected. In the final axial and lateral strain images (h,n), the inclusions are easily detectable and it is worth noting that these inclusions are less deformed than the surrounding medium, which perfectly reflects a stiffer area. Concerning the shear strain (k), the improvement is weaker than for the lateral strain, and compared with the simulation (l) the field presents some line artefacts along the lateral direction. These artefacts are mainly induced by the differentiation of the lateral displacement field along the axial direction. A 8×2 median filter was applied to this field before shear computation, which reduces but not completely annihilates them. Nevertheless, (k) shows similar patterns to (l) and the presence of the inclusions can be detected. Finally, it is important to highlight that, although our method is a 2D approach, the regularized strain fields are consistent with a medium deforming in 3D.

The results obtained with breast tissues are now presented using archived data from a previous breast elastography study, which was approved by the local ethics committee (case #3, Fig. 1c, Fig. 4). Detailed information about this study can be found in [18]. It should be underlined that data acquisition was conducted similarly to that described above. The case selected is one of an invasive ductal carcinoma (IDC). Once again, the regularization effect on the axial displacement (a-b) and strain (e-f) remains limited, while it drastically improves the lateral components (c-d, i-j). In both axial and lateral regularized strain fields, the abnormal area is perfectly distinguishable and appears stiffer than

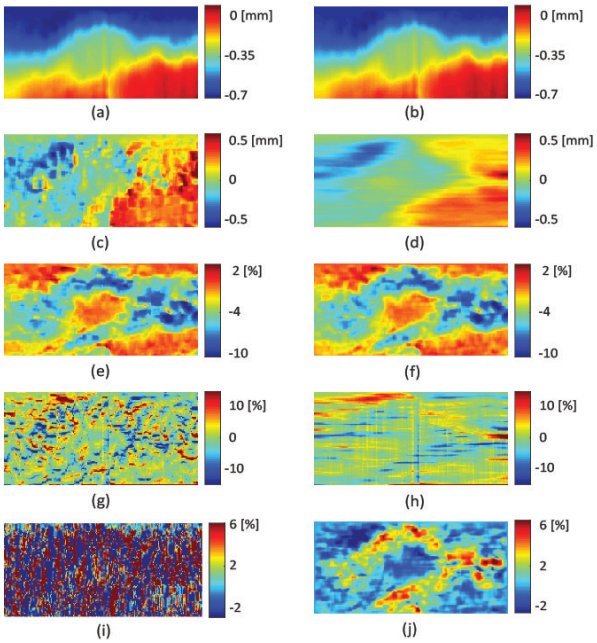

Fig. 4. Breast tissue results with an abnormal area corresponding to an IDC - case #3. From top to bottom: axial displacement, lateral displacement, axial strain, shear strain, and lateral strain. Fields obtained before (left) and after (right) regularization. A 8×2 median filter was used in (g) and (h).

the surrounding tissues, which is in agreement with the observations generally made for IDCs in elastography studies. Further analysis is nonetheless difficult, due to the high complexity of biological media and the lack of information regarding the mechanical properties of the examined tissues, which also prevent any simulations from being performed.

Finally, the CNR is calculated to provide a more quantitative metric to assess the performance of the proposed method. The CNR is widely employed in elastography studies as an indicator of lesion detectability within an image. It is computed as follows :

$$CNR = \sqrt{\frac{2(\bar{s}_i - \bar{s}_b)^2}{\sigma_i^2 + \sigma_b^2}} \tag{3}$$

where $\bar{s}$ and σ denote the mean and the standard deviation of the strain, respectively, within a region inside the inclusion (subscript i) and the background (subscript b). These regions are selected using two circular ROIs of identical size and positioned at the same depth. For each inclusion, two CNRs are computed, one by selecting the background region on the right of the inclusion (Fig. 5a) and the other one on the left (Fig. 5b). The multiplying factor (MF) is also calculated as the ratio of CNRs after and before the regularization. The results are presented in Table I.

We can directly point out that the results support the above visual observations for both phantoms (case #1 and case #2) and *in vivo* breast tissues (case #3). More precisely, $\text{CNR}_{lateral}$ significantly improved with the regularization,

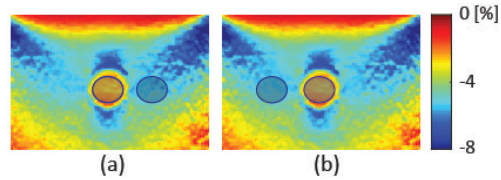

Fig. 5. Illustration of the two configurations for ROI selection with the axial strain image, case #1 (Fig. 2g).

with values in the range [0.68 - 9.40] vs [0.09 – 0.38] before regularization. It is also interesting to note that $\text{CNR}_{lateral}$ values after regularization are quite close to CNR_{axial} ones, which confirms that the inclusions/lesion are now as easily detectable in the lateral strain images as they are in the axial ones. A specific comment can be made for the bottom inclusion in case #2, which shows more variations in the results than the other cases. For this inclusion, the multiplying factor is extremely different, 2.16 and 34.86, depending on where the background region is selected. This difference is due to the higher heterogeneity in the strain values for the region selected on the right of the inclusion. Concerning the axial strain, we showed that the regularization process has no visible impact on these fields. For all that, a slight improvement in CNR_{axial} can be observed, with a multiplying factor ranging from 1.04 to 1.15.

IV. CONCLUSION

In this paper, 2D strain tensor imaging was investigated involving the use of a specific regularization method. Results show the strong contribution of this regularization when facing complex and noisy data, especially for the lateral displacement and strain fields. Beyond a more complete analysis of the medium strain, these results are particularly interesting for mechanical parameter reconstruction. These are, however, only preliminary results and future work will focus on a more thorough assessment of the proposed method, but also on the introduction of modifications to still improve the results, especially the shear strain.

REFERENCES

[1] J. Ophir, I. Céspedes, H. Ponnekanti, Y. Yazdi, and X. Li, "Elastography: a quantitative method for imaging the elasticity of biological tissues," *Ultrasonic Imaging*, vol. 13, pp. 111–134, 1991.

[2] P. Wells and H. D. Liang, "Medical ultrasound: imaging of soft tissue strain and elasticity," *Journal of The Royal Society Interface*, vol. 8, pp. 1521–1549, 2011.

[3] S. Venkatesh, M. Yin, and R. Ehman, "Magnetic resonance elastography of liver: Technique, analysis, and clinical applications," *Journal of Magnetic Resonance Imaging*, vol. 37, pp. 544–555, 2013.

[4] H. Xu and T. Varghese, "Normal and shear strain imaging using 2D deformation tracking on beam steered linear array datasets," *Medical Physics*, vol. 40, p. 012902, 2013.

[5] G. Hendriks, C. Chen, H. Hansen, and C. de Korte, "3-D Single Breath-Hold Shear Strain Estimation for Improved Breast Lesion Detection and Classification in Automated Volumetric Ultrasound Scanners," *IEEE Transactions on Ultrasonics, Ferroelectrics, and Frequency Control*, vol. 65, pp. 1590–1599, 2018.

[6] B. Friemel, L. Bohs, and G. Trahey, "Relative performance of two-dimensional speckle-tracking techniques: normalized correlation, non-normalized correlation and sum-absolute-difference," in *1995 IEEE Ultrasonics Symposium. Proceedings*, vol. 2, pp. 1481–1484, 1995.

TABLE I

CONTRAST-TO-NOISE RATIOS (CNRS) BEFORE AND AFTER REGULARIZATION, AND THE CORRESPONDING MULTIPLYING FACTORS (MFS)∗.

	CNR_{axial}			$CNR_{lateral}$		
	Before Reg.	After Reg.	MF	Before Reg.	After Reg.	MF
Case #1 - right	9.38	10.07	1.07	0.35	9.40	26.47
Case #1 - left	10.51	11.19	1.06	0.35	8.82	24.93
Case #2 - top right	7.57	7.89	1.04	0.27	5.54	20.32
Case #2 - top left	7.09	7.81	1.10	0.38	5.84	15.33
Case #2 - bottom right	2.20	2.30	1.04	0.31	0.68	2.16
Case #2 - bottom left	3.76	3.98	1.06	0.09	3.25	34.86
Case #3 - right	4.12	4.73	1.15	0.10	2.17	21.95
Case #3 - left	5.64	6.10	1.08	0.18	3.01	16.40

∗For each of the three cases considered, CNRs and MFs are calculated by selecting the background region on the right (Fig. 5a) or on the left (Fig. 5b) of the inclusion. For case #2, CNR values are provided for each of the two inclusions.

[7] K. Liu, P. Zhang, J. Shao, X. Zhu, Y. Zhang, and J. Bai, "A 2D strain estimator with numerical optimization method for soft-tissue elastography," *Ultrasonics*, vol. 49, pp. 723–732, 2009.

[8] J. F. Deprez, E. Brusseau, C. Schmitt, G. Cloutier, and O. Basset, "3D estimation of soft biological tissue deformation from radio-frequency ultrasound volume acquisitions," *Medical Image Analysis*, vol. 13, pp. 116–127, 2009.

[9] M. M. Doyley, "Model-based elastography: a survey of approaches to the inverse elasticity problem," *Physics in Medicine and Biology*, vol. 57, pp. R35–R73, 2012.

[10] U. Techavipoo, Q. Chen, T. Varghese, and J. Zagzebski, "Estimation of Displacement Vectors and Strain Tensors in Elastography Using Angular Insonifications," *IEEE Trans Med Imaging*, vol. 23, pp. 1479–1489, 2004.

[11] H. Liebgott, J. Fromageau, J. Wilhjelm, D. Vray, and P. Delachartre, "Direct estimation of the lateral strain field using a double oscillating point spread function with a scaling factor estimator," *Proc. of SPIE Medical Imaging*, vol. 5373, pp. 163–172, 2004.

[12] E. Konofagou and J. Ophir, "A new elastographic method for estimation and imaging of lateral displacements, lateral strains, corrected axial strains and Poisson's ratios in tissues," *Ultrasound in Medicine & Biology*, vol. 24, pp. 1183–1199, 1998.

[13] Z. Hu, H. Zhang, J. Yuan, M. Lu, S. Chen, and H. Liu, "An H∞ Strategy for Strain Estimation in Ultrasound Elastography Using Biomechanical Modeling Constraint," *PLoS ONE*, vol. 8, p. e73093, 2013.

[14] H. Rivaz, E. Boctor, M. Choti, and G. Hager, "Real-Time Regularized Ultrasound Elastography," *IEEE Transactions on Medical Imaging*, vol. 30, pp. 928–945, 2011.

[15] R. Al Mukaddim, N. H. Meshram, and T. Varghese, "Locally optimized correlation-guided Bayesian adaptive regularization for ultrasound strain imaging," *Physics in Medicine and Biology*, vol. 65, p. 065008, 2020.

[16] L. Guo, Y. Xu, Z. Xu, and J. Jiang, "A PDE-based regularization algorithm toward reducing speckle tracking noise: a feasibility study for ultrasound breast elastography," *Ultrasonic Imaging*, vol. 37, pp. 277–293, 2015.

[17] M. Lubinski, S. Emelianov, K. Raghavan, A. Yagle, A. Skovoroda, and M. O'Donnell, "Lateral displacement estimation using tissue incompressibility," *IEEE Transactions on Ultrasonics, Ferroelectrics and Frequency Control*, vol. 43, pp. 247–256, 1996.

[18] E. Brusseau, V. Detti, A. Coulon, E. Maissiat, N. Boublay, Y. Berthezène, J. Fromageau, N. Bush, and J. Bamber, "In Vivo Response to Compression of 35 Breast Lesions Observed with a Two-Dimensional Locally Regularized Strain Estimation Method," *Ultrasound in Medicine & Biology*, vol. 40, pp. 300–312, 2014.

[19] E. Brusseau, J. Kybic, J. F. Deprez, and O. Basset, "2-D Locally Regularized Tissue Strain Estimation From Radio-Frequency Ultrasound Images: Theoretical Developments and Results on Experimental Data," *IEEE Transactions on Medical Imaging*, vol. 27, pp. 145–160, 2008.

[20] "Comsol Multiphysics® v. 5.5, `http://www.comsol.com`, COMSOL AB, Stockholm, Sweden."